PHYSOR 2014 - The Role of Reactor Physics toward a Sustainable Future
The Westin Miyako, Kyoto, Japan, September 28 - October 3, 2014, on CD-ROM (2014)

INVENTORY UNCERTAINTY QUANTIFICATION AND PROPAGATION USING TENDL COVARIANCE DATA IN FISPACT-II

James W. Eastwood and J. Guy Morgan*
Culham Electromagnetics Ltd
Culham Science Centre, Abingdon OX14 3DB, United Kingdom
James.Eastwood@Culhamem.co.uk
Guy.Morgan@Culhamem.co.uk

Jean-Christophe C. Sublet†
United Kingdom Atomic Energy Authority
Culham Science Centre, Abingdon OX14 3DB, United Kingdom
jean-christophe.sublet@ccfe.ac.uk

ABSTRACT

The new inventory code FISPACT-II provides predictions of inventory, radiological quantities and their uncertainties using nuclear data covariance information. Central to the method is a novel fast pathways search algorithm using directed graphs. The pathways output provides (1) an aid to identifying important reactions, (2) fast estimates of uncertainties, (3) reduced models that retain important nuclides and reactions for use in the code's Monte-Carlo sensitivity analysis module. Described are the methods that are being implemented for improving uncertainty predictions, quantification and propagation using the covariance data that the recent nuclear data libraries contain. In the TENDL library, above the upper energy of the resolved resonance range, a Monte Carlo method in which the covariance data come from uncertainties of the nuclear model calculations is used. The nuclear data files are read directly by FISPACT-II without any further intermediate processing. Variance and covariance data are processed and used by FISPACT-II to compute uncertainties in collapsed cross-sections, and these are in turn used to predict uncertainties in inventories and all derived radiological data.

Key Words: **Numerical Modelling, Graph Theory, Activation, Transmutation, Uncertainty, Sensitivity, Covariance**

1. Introduction

FISPACT-II[1, 2] is the new inventory code central to the EASY-II system[3]. It was developed by the authors of this paper originally as a functional replacement for Fispact-2007[4], but now has substantially extended capabilities (c.f., Section 2).

*http://www.culhamem.co.uk
†http://www.ccfe.ac.uk/EASY.aspx

This paper focuses on the novel treatment of pathways and uncertainty in the new code. The pathways analysis (Section 3) is used to identify the most significant chains of reactions and decays in transmuting the initial inventory to the dominant nuclides at the end of a chosen step. Section 4 summarises how estimates of uncertainty are computed using the uncertainties in the cross-sections and decay constants for nuclides on these significant chains. Section 5 outlines a more complete Monte-Carlo treatment of uncertainties where covariance data are used to find independent input uncertainties and pathways help reduce the problem size. Section 6 demonstrates the system capabilities in comparing experimental measurements of decay heat with their associated experimental uncertainty with simulation results also associated with their calculational uncertainty.

2. FISPACT-II

2.1. Capabilities

FISPACT-II is a practical activation-transmutation engineering prediction tool. It automatically accommodates given nuclear data libraries by using dynamical memory allocation. The four main tasks that it undertakes are

1. extraction, reduction and storage of nuclear, radiological data and covariance from the EAF or ENDF library files;
2. construction and solution of the rate equations to determine the time evolution of the inventory in response to different irradiation scenarios. These scenarios include
   (a) a cooling-only calculation;
   (b) a single irradiation pulse followed by cooling;
   (c) multiple irradiation pulses where only flux amplitudes change, followed by cooling;
   (d) multi-step irradiation where flux amplitude, flux spectra and cross-sections may change, followed by cooling.
3. computation and output of derived radiological quantities;
4. subsidiary calculations to identify the key reactions and decays, and to assess the quality of the predictions. The four main subsidiary items are
   (a) pathways analysis;
   (b) uncertainty calculations from pathways;
   (c) reduced model calculations;
   (d) Monte-Carlo sensitivity and uncertainty calculations.

The current version (2.1) of the code can undertake pathways and sensitivity calculations for multi-pulse irradiation cases. Self-shielding may be included in the cross-section collapse calculations

using either CALENDF [5] probability table data or the universal curve model[6] associated with TENDL ENDF file 2 data. The code uses the EAF-2010[7], TENDL-2011 or TENDL-2012[8] libraries for its nuclear data. With the TENDL libraries, it handles more irradiating projectiles (γ, n, p, d, α), provides additional diagnostic outputs (kerma, dpa and gas appm rates) and uses cross-section covariance data.

2.2. Data Collapse

The TENDL libraries[9] provide cross-sections X_i, Y_j and (by projection) covariances $cov(X_i, Y_j)$ in energy bins i, j. The EAF libraries provide cross-sections and their fractional uncertainties only. Flux (ϕ_i) weighted collapsed values used by FISPACT-II are given by

$$\bar{X} = \sum_i W_i X_i \; ; \quad cov(\bar{X}, \bar{Y}) = \sum_{ij} W_i W_j cov(X_i, Y_j) \tag{1}$$

where $W_i = \phi_i / \sum_j \phi_j$ and the sums are over all energy bins.

The covariance data in the EAF or TENDL-2011 and TENDL-2012 libraries that FISPACT-II recognises are the ENDF [10] NI-type data with LB=1, 5, or 6. Covariance data are stored as fractional values $F_{kk'}$ in wide energy bins and values are mapped using projection operators S_i^k, where $S_i^k = 1$ if energy bin i overlaps bin k, and is zero otherwise as illustrated in Figure 1.

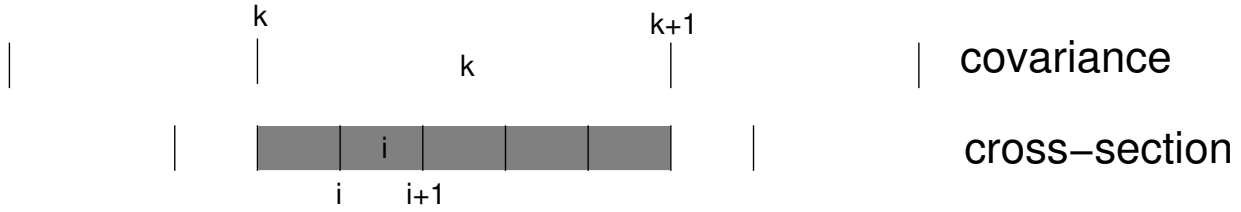

Figure 1. Projection operator S_i^k maps cross-section energy bins to covariance energy bins. The shaded energy bins have $S_i^k = 1$, and all others have $S_i^k = 0$.

Using S_i^k, the formulae used to construct estimates of the covariance matrix from the library data are as follows:

$$LB = 1: \quad Cov(X_i, X_j) = \sum_{k=1}^{K} S_i^k S_j^k F_k X_i X_j \tag{2}$$

$$LB = 5: \quad Cov(X_i, Y_j) = \sum_{k=1}^{K} \sum_{k'=1}^{K} S_i^k S_j^{k'} F_{kk'} X_i Y_j \tag{3}$$

$$LB = 6: \quad Cov(X_i, Y_j) = \sum_{k=1}^{K} \sum_{k'=1}^{K'} S_i^k S_j^{k'} F_{kk'} X_i Y_j \tag{4}$$

where K and K' respectively are the number of covariance data energy bins for cross-section data X_i and Y_j. FISPACT-II computes collapsed covariances by substituting Equations (2)-(4) in Equation (1) as appropriate. Fission yield data are treated in a similar fashion.

3. Pathways Analysis

The inventory of a given nuclide computed using the rate equations may equivalently be found by a superposition of contributions of flows along a network of pathways to that nuclide, where a pathway is the combination of a linear chain of reactions between different nuclides (a path), plus a number of loops from a nuclide to itself. Pathways analysis finds the significant pathways by automatically combining paths and loops, and these pathways are used in performing uncertainty and sensitivity calculations.

Source nuclides for the pathways calculation are the initial inventory, and target nuclides are dominant nuclides at the current timestep. A dominant nuclide is one that gives a major contribution to a radiological quantity, such as activity, gamma dose, heating, inhalation dosage, etc.

Brute-force searching for pathways rapidly fails owing to the combinatorial growth of possibilities. The novel graph-theoretic algorithm we have developed[11, 12] leads to faster and lower-storage computations. Our algorithm for finding pathways, implemented using linked-list queues, is

1. create a single-visit digraph with edge-weight pruning;
2. iterate on the digraph to extract all edges on significant paths and loops;
3. use these edges to build a tree with weight, loop and depth pruning;
4. combine resulting paths and loops to make pathways;
5. compute inventories along pathways and discard those below a user-specified threshold.

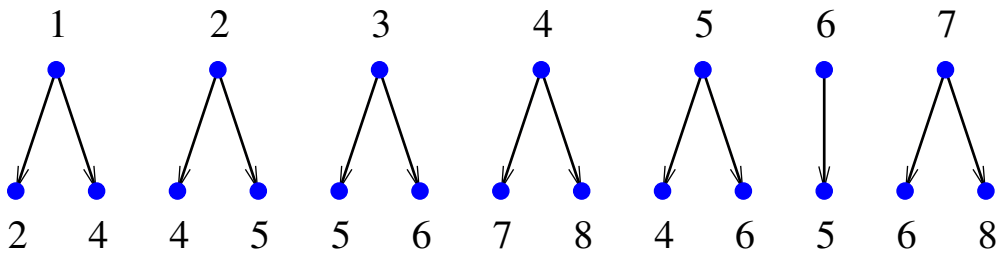

Figure 2. Adjacency list for the 8-nuclide example.

To illustrate the method we consider the eight nuclide example whose adjacency list is shown in Figure 2. Parent 1 has daughters 2 and 4, etc. To find paths originating at nuclide 1, a single-visit tree is built breadth-first (Figure 3). At the second level, children of 2 (4 and 5) and 4 (7 and 8) are added. At the third level, children of 4 are not added because nuclide 4 has already been visited as a parent at level 1 and only the first occurrence of nuclide 6 has its children added. The tree is completed at level 4. All the leaves of the tree are nuclides that have appeared earlier.

Graph edges are extracted from the digraph of Figure 3 by iteration. Consider for example paths from nuclide 1 to 4. At the first iteration, edges with nuclide 1 or 4 as children are extracted, giving edges (14), (24) and (54), and adding target nuclides 2 and 5. At the next iteration, edges with

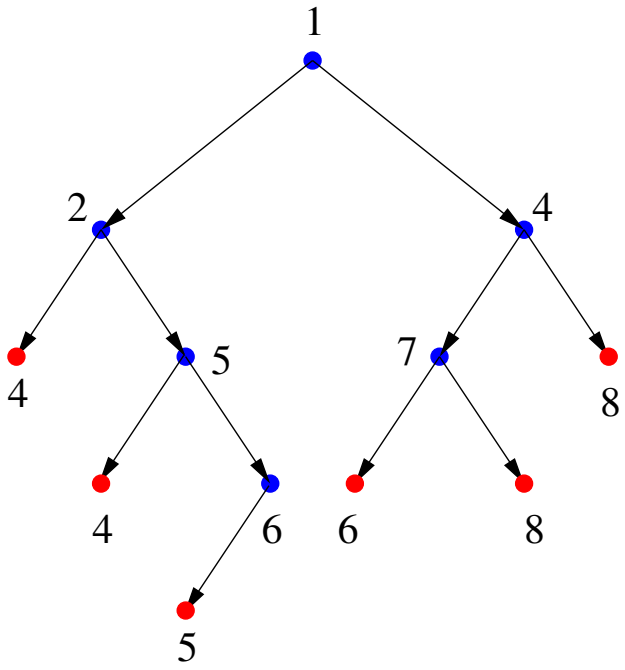

Figure 3. A parent single-visit tree for nuclide 1.

children 2 and 5 are extracted, giving edges (12), (25) and (65), and target 6. The third iteration gives (56) and (76) and target 7. The final iteration finds edge (47) and introduces no further target nuclides so the iteration terminates.

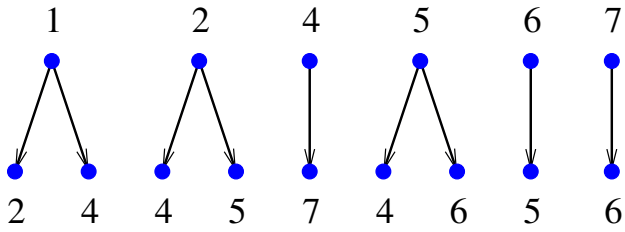

Figure 4. Adjacency list for pathways between nuclides 1 and 4.

Figure 4 shows the set of edges that are involved in pathways from nuclide 1 to 4. If we excluded pathways with loops on the final nuclide (4), then branches of the full tree could be terminated at occurrences of nuclide 4. Instead, we collect paths and loops separately, and use the following criteria to terminate branches:

1. a loop is found (i.e., a nuclide is encountered that has already occurred on the path from the root to the leaf);
2. the leaf has a weight below the path floor value;
3. the depth exceeds the maximum depth.

In Figure 5, the solid red line shows a branch terminated by criterion 1, and the broken lines show branches terminated by criterion 2. Traversing the tree reveals paths 1-4, 1-2-4 and 1-2-5-4 at levels 1, 2 and 3, and loop [56] at level 4.

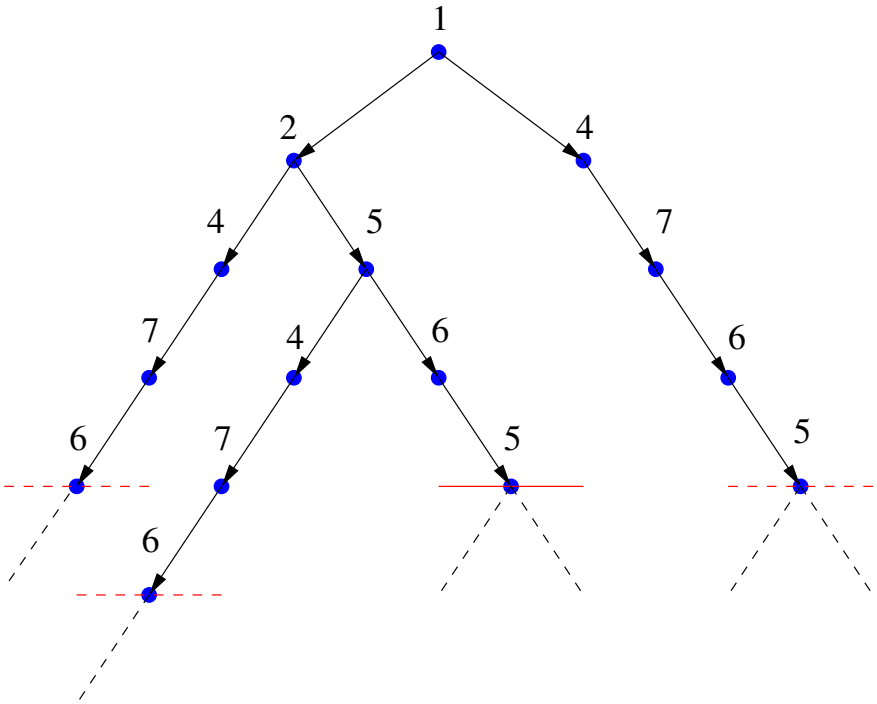

Figure 5. The breadth-first tree for the adjacency list of Figure 4.

The pruning weight criteria (Section 3.1 below) are sufficient conditions for a pathway to be discarded. The final list is found by integrating the rate equations along the pruned list and discarding those below the chosen thresholds. Figure 6 shows the pathways found.

Loops are discarded if they increase the inventory of a path by less that the loop floor fraction. The weights for discarding paths are discussed in the section below.

Note in this example if we had a smaller path floor, then the loop [5476] would have been found and would have been combined with the paths shown in Figure 6 if its contribution exceed the loop floor criterion.

3.1. Threshold pruning

Pathways are assigned importance based on the fractions of the inventory at the target nuclide that come via them from the source nuclide. Each intermediate step i from nuclide i to $i+1$ along a dominant pathway between the source and the target introduces a reduction in the flow that can be bounded by a reduction factor less than unity.

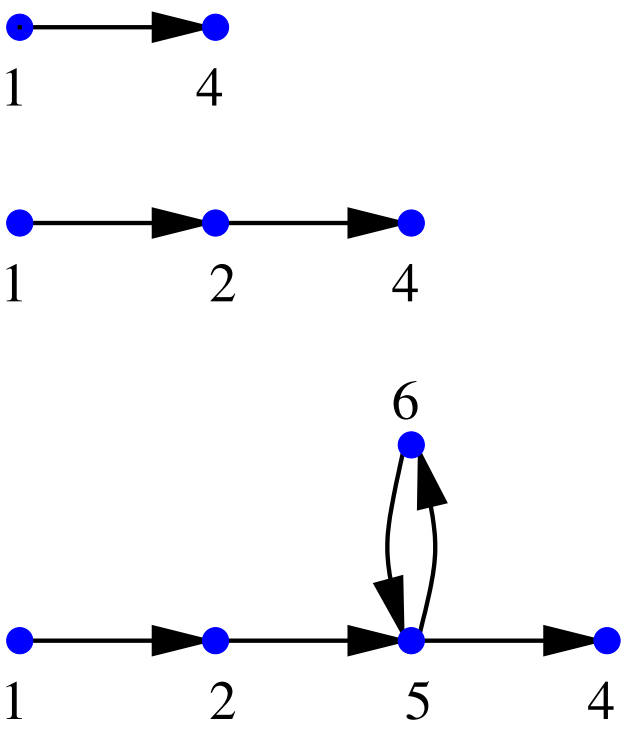

Figure 6. The pathways obtained from the tree in Figure 5.

If N_s and N_t are respectively the initial number of source atoms and the final number of target atoms given by the full inventory calculation, and ϵ is the threshold fraction of N_t below which the pathway is not considered significant, then any partial pathway with inventory N_D at depth D for which

$$\rho_D = N_D/N_s < \epsilon N_t/N_s \tag{5}$$

can be pruned. Estimated bounds on ρ_D can be found from the rate equation coefficients and the time interval being considered, but the final pruning and pathway assessment will require integration of the inventory along the pathway.

An upper bound for ρ_i at level i can be found by considering the flow along the linear chain that forms a path. The evolution of the inventory is given by

$$\frac{dN_1}{dt} = -\alpha_1 N_1 \tag{6}$$

and for subsequent nuclides ($i > 1$)

$$\frac{dN_i}{dt} = -\alpha_i N_i + \beta_{i-1} N_{i-1} \tag{7}$$

where α_i gives the total rate of decay and induced destruction of a nuclide, and β_i is the rate of decay and transmutation of nuclide i specifically to nuclide $i+1$.

For constant flux, α_i and β_i are constant, so Equation (7) may be integrated to give

$$N_i(t) = e^{-\alpha_i t}\left(A_i + \int_0^t e^{\alpha_i t'}\beta_{i-1}N_{i-1}(t')dt'\right) \tag{8}$$

where for $i > 1$, the initial conditions give $A_i = 0$.

The total number of nuclides created at vertex $i+1$ in time interval $[0, T]$ is

$$F_{i+1} = \int_0^T \beta_i N_i dt \tag{9}$$

Substituting Equation (8) into Equation (9), interchanging the order of integration and integrating over t gives

$$\begin{aligned} F_{i+1} &= \frac{\beta_i}{\alpha_i}\left(F_i - e^{-\alpha_i T}\int_0^T dt'\ N_{i-1}(t')\beta_{i-1}e^{\alpha_i t'}\right) \\ &\leq \frac{\beta_i}{\alpha_i}F_i(1-e^{-\alpha_i T}) \end{aligned} \tag{10}$$

where the final inequality was obtained by replacing the exponential in the integral by its lower bound ($= 1$) in Equation (10).

Setting $F_1 = 1$ and computing F_{i+1} using the inequality in Equation (10) gives an upper bound on ρ_i, and so provides a sufficient pruning condition for terminating branches in trees such as that illustrated in Figure 5.

The tree-pruning criterion for a single pulse of irradiation may be extended to multi-pulse irradiation of J pulses by replacing F by a vector of length J. A sufficient condition for the pathway to be discarded at depth D (> 0) is

$$F_{D+1}(T_J) < \epsilon\frac{N_t(T)}{N_s(0)} \tag{11}$$

where this inequality is applied only to the final components of the vectors F at time T_J. The total fluxes satisfy initial conditions

$$F_i(T_0) = 0; \quad i > 1 \tag{12}$$

and at the end of time interval j (> 0)

$$\begin{aligned} F_{i+1}(T_j) &\leq F_{i+1}(T_{j-1}) \\ &+ \frac{\beta_i^j}{\alpha_i^j}F_i(T_j)[1-\exp(-\alpha_i^j\Delta T_j)] \end{aligned} \tag{13}$$

where $\alpha_i^j > 0$, $F_1(T_j) = N_{1,j-1}$ and $\Delta T_j = T_j - T_{j-1}$.

Pruning weights using Equations (10)-(13) are implemented in the FISPACT-II pathways calculations. The parameter ϵ for pruning paths and the corresponding parameter for retaining loops on a pathway may be controlled by two input parameters available to users of FISPACT-II:

path_floor {0.005} All pathways contributing more than the *path_floor* fraction of the inventory of the final (target) nuclide are retained.

loop_floor {0.01} All loops that increase the inventory contribution of the path they are on by a fraction greater than the *loop_floor* are retained.

where the numbers in the brackets are default values used by the code. Making them smaller makes little change to the error estimates and will increase the computation times. The default values generally capture paths that account for over 99% of the total inventory at the target nuclide.

4. Uncertainty Estimates

The pathways, the number of atoms created at target nuclide t due to the reaction and decay chain along path p to that nuclide together with uncertainties in the reaction cross-sections and decay half lives associated with the edges of the pathways are used in FISPACT-II to provide estimates of the uncertainties.

The approach used is a generalisation of that used in FISPACT 2007[4]. Pathways arising from a fission are assumed to be correlated and their uncertainties are summed. All other pathway contributions are treated as uncorrelated and are combined in a random walk approximation. The uncertainty contributions from the reactions along the edges of each pathway are also combined using random walks. If only variances of cross-sections are known, then the cross-sections are assumed to be uncorrelated. If covariance data are known for cross-sections, then the independent variables are obtained by diagonalising the covariance matrix. In deriving the formulae used in FISPACT-II it is also assumed that the number of nuclides formed along path p of length n to target nuclide t at time T

$$N_{tp} = N_{10} \left(\prod_{i=1}^{n-1} \beta_i \right) \sum_{i=1}^{n} e^{-\alpha_i T} / \prod_{\substack{j=1 \\ j \neq i}}^{n} (\alpha_i - \alpha_j) \tag{14}$$

may be approximated by

$$N_{tp} = C_{tp} \prod_{i=1}^{n-1} \beta_i \tag{15}$$

where C_{tp} is a constant for path p to target t..

Given a set of target nuclides S_t, then the uncertainty in some radiological quantity $Q = \sum_{t \in S_t} q_t$ is given by ΔQ, where

$$(\Delta Q)^2 = \sum_{t \in S_t} \left(\frac{\Delta N_t}{N_t} \right)^2 q_t^2 \tag{16}$$

N_t is the number of atoms of target nuclide t formed from the initial inventory and ΔN_t is the error in N_t. N_t and q_t are known from the inventory calculation. ΔN_t is computed from the pathways inventories and the fractional squared error Δ_{tp}^2 in the number of atoms of target nuclide t formed along pathway p to that target. Only those error contributions coming through the dependence on N_t are included in the present implementation.

If we let the set of pathways to target t be S_p, then $S_p = (\cup_{a \in S_{sa}} S_a) \cup S_o$ where S_a is the subset of these pathways that start from the fission of an actinide source nuclide a and S_o is the set of other pathways. S_{sa} is the subset of the set of source nuclides that are actinides.

If all the pathways to a target nuclide t are uncorrelated, then the uncertainty in the inventories along pathways p to t can be combined using a random walk approximation to give an estimate of the uncertainty of the target nuclide inventory ΔN_t:

$$(\Delta N_t)^2 = \sum_p (\Delta N_{tp})^2 \tag{17}$$

However, pathways arising from a fission are correlated and so are combined linearly:

$$\Delta N_t = \sum_p \Delta N_{tp} \tag{18}$$

Combining these gives the expression for the total ΔN_t

$$(\Delta N_t)^2 = \sum_{p \in S_o} \Delta N_{tp}^2 + \sum_{a \in S_{sa}} \left(\sum_{p \in S_a} |\Delta N_{tp}| \right)^2 \tag{19}$$

If we treat each cross-section as independent, then on edge e of a pathway, $\beta_e = \sigma_e = \sum_r \sigma_r$, and so from Equation (15), the contribution of reaction r on edge e is

$$\delta \left(\frac{\Delta N_{tp}}{N_{tp}} \right) = \frac{\Delta \sigma_r}{\sigma_e} \tag{20}$$

If there are off-diagonal covariance matrix terms for the cross-sections, the independent variables are found by diagonalising the covariance matrix. Let reaction r belong to the set of reactions $\{X_1 \dots X_D\}$ for a parent where $cov(X_i, X_j)$ are nonzero for $i \neq j$, then we can find a similarity transformation matrix M such that $cov(Y, Y) = M^T cov(X, X) M$ is diagonal with diagonal elements $var(Y)$, and $Y = M^T X$. Components of Y are the independent variables, and from Equation (15) the contribution to the uncertainty of inventory N_{tp} becomes

$$\delta \left(\frac{\Delta N_{tp}}{N_{tp}} \right) = \frac{M_{i(r)j} \Delta Y_j}{\sigma_e} \tag{21}$$

where the dependence of index i on reaction r is indicated.

Using the random walk assumption and ignoring any off-diagonal covariance matrix terms gives

$$\begin{aligned} \Delta_{tp}^2 &= \left(\frac{\Delta N_{tp}}{N_{tp}} \right)^2 \\ &= \sum_{e,r} \left(\frac{\Delta \sigma_r}{\sigma_e} \right)^2 + \sum_{e \in D_e} \left(\frac{\Delta \tau_j}{\tau_e} \right)^2 \end{aligned} \tag{22}$$

where the first sum is over all edges e on each pathway p, all reactions r on each edge and over all $\Delta Y_j = \sqrt{var(Y_j)}$ from the diagonalised covariance matrix for reaction r. The second term gives the contribution of decay constant uncertainties and is summed over the set of edges as defined in the

FISPACT 2007 manual[4]. Equation (22) is generalised to handle multi-pulse irradiation scenarios by replacing the first term by

$$\sum_{e,r} \left(\frac{R_r(\Delta\sigma_r/\sigma_r)}{R_e} \right)^2$$

where R_r and R_e are respectively the pulse averaged reaction rates of reaction r and the pulse averaged reaction rate on edge e.

In FISPACT-II, the pulse-averaged fractional squared errors Δ^2_{tp} are precomputed from the nuclear data and are used in conjunction with values of N_{tp} from pathways calculations and N_t from the main inventory calculation to provide error estimates throughout a calculation.

5. Sensitivity Calculation

5.1. Monte-Carlo

FISPACT-II uses a Monte-Carlo approach to sensitivity analysis. A series S of inventory calculations is performed with the set of I independent variables $\{X_i^s;\ i = 1, \ldots, I;\ s = 1, \ldots, S\}$ chosen from distributions with means $\langle X_i \rangle$ and standard deviations $\langle \Delta X_i \rangle$. These runs produce a set of J dependent variables $\{Q_j^s;\ j = 1, \ldots, J;\ s = 1, \ldots, S\}$. For the EAF libraries, the cross-sections are treated as the independent variables, but with the TENDL libraries it is possible to take into account covariance data to get a more complete assessment of the uncertainties of results.

The TENDL libraries contain covariance data between some reactions of given parents[9]. FISPACT-II reads these data and collapses the covariances as described in Section 2. Given a rank D symmetric positive definite covariance matrix, we can find a $D \times D$ similarity transformation matrix M such that $Y = M^T X$ and $cov(Y, Y) = M^T cov(X, X) M$ is diagonal with diagonal elements $var(Y)$. The transformed cross-sections Y are treated as the independent variables, and random samples with means $\langle Y_i \rangle$ and standard deviations $\langle \Delta Y_i \rangle$ are chosen, and the input sample cross-sections are computed using $X = MY$.

The dependent variables are the numbers of atoms of nuclides j or some related radiological quantity. The pathways summaries created by pathways analysis provide a good guide as to which cross-sections and decays are likely to be important to include as independent variables in the sensitivity calculation.

Selecting a sensitivity calculation in FISPACT-II causes the series of S runs with different independent variables to be undertaken to compute, process and output the set $\{Q_j^s\}$. The default independent variable distribution is taken to be log-normal, but other options are provided (normal, log-uniform and uniform). Any sequence of irradiation pulses, changes in cross-section, etc. that are possible with FISPACT-II can be used in the sensitivity calculations. The code performs the base calculation with full output, then repeats S times the sequence of steps with different sets $\{X_i^s\}$. The results of the base calculation are not included in the sensitivity calculation.

Sensitivity calculations provide both uncertainty and sensitivity output. Summary uncertainty output of means $\bar{X}_i$ and $\bar{Q}_j$ and standard deviations ΔX_i and ΔQ_j is produced. The code writes tables of means, standard deviations and Pearson correlation coefficients, and outputs the raw data $\{X_i^s,\ Q_j^s;\ i = 1, \ldots, I;\ j = 1, \ldots, J;\ s = 1, \ldots, S\}$ to file for possible post-processing.

5.2. Model Reduction

FISPACT-II usually runs with the full TENDL-2012 library of 2429 targets and 3873 daughter products and decays that are included in the library. Nuclides that are present in the master nuclide index used by the code are included in a calculation. For single inventory calculations, the cpu time used is small, with the dominant time often being that taken to read and collapse the 9 Gigabytes of ASCII data in the TENDL-2012 library.

FISPACT-II has the capability to produce a reduced index in a pathways inventory run, where only those nuclides that appear on pathways from the initial inventory to the dominant nuclides are included. Using a reduced index leads to much faster library reading. Memory allocation in the code is all dynamic, and so calculations with a reduced number of nuclides in the index also use less memory.

Sensitivity calculations can also benefit from the model reduction capability. Pathways analysis identifies the important nuclides and reactions. The code has the capability of outputting a reduced master index that includes only those nuclides that appear on the pathways. Repeating calculations using this reduced master index usually accurately reproduces the results from the full calculation. Monte-Carlo sensitivity calculations using the reduced master index will retain the important reactions and decays but will demand smaller cpu time and memory resources. typical speed-up factors of 10^4 without any significant loss of accuracy have been found in some Monte-Carlo validation tests.

6. Verification and Validation

Careful software lifecycle management under configuration control has been used for the code, unit and integration tests and verification tests. EASY-II is distributed with over 400 input/output regression tests that preserve and extend the verification-validation heritage of EASY-2010 and its predecessors [3].

Figure 7 is an example from a validation study against experimental results [13] where experimental results were compared against simulated integral values. The experiment was the JAEA FNS assembly where 14 MeV neutrons were generated by a 2 mA deuteron beam impinging on a stationary tritium bearing titanium target has proven most beneficial [14].

More than seventy different material samples have been irradiated in sequence to have their decay heat measured in a whole energy absorption spectrometer. The value of those integral results reside mainly in the well characterized and stable neutron spectra at the target position, but also in the time

scale of the measurements from a few seconds after irradiation up to 400 days. All experimental results have been compared with values derived from the EASY-II simulation. For both calculated and experimental values uncertainty estimates are also provided.

The FISPACT-II simulations used the radom-walk approximation uncertainty estimate methods described in Section 4, where only the covariance data in the TENDL-2012 library between different energy groups $Cov(X_i, X_j)$ of reaction X were used. All covariance data between different reactions were ignored.

Figure 7 demonstrates the validation results for two samples of Yttrium oxide irradiated for 5 minutes and 7 hours at JAEA FNS. Decay heat and its associated uncertainty were measured for both samples at many cooling time ranging from 36 s to 400 days. The short term decay heat is well predicted, as the calculational uncertainties (grey areas) compare with the experimental (vertical bar) ones. However, the code prediction seems to underestimate the long term one by around 20%, but it is worth noting that the predicted uncertainty, the grey area, still encompasses the experimental data points.

7. Final Remarks

FISPACT-II brings new capabilities to the long established family of activation codes. At its core is a rate-equation solver that exploits the nuclear data from the EAF, TENDL or any ENDF formatted libraries. It has a powerful pathways analysis capability that can easily identify dominant nuclides and significant reaction and decay pathways, so providing a reduced set of odes that capture most of the physics. This reduced set could then be used as the basis of conventional sensitivity analysis using direct or adjoint methods. Instead, in our work we have focused on a practical engineering tool that provides fast uncertainty estimates in activation calculations that may involve multiple pulse irradiation follow by a cooling period. The code also provides a more computationally intensive Monte-Carlo approach (c.f., Section 5) that allows the random-walk error estimate to be cross-checked in important cases for complex irradiation/cooling scenarios without using the simplifying assumptions outlined in Section 4.

This paper has introduced the methods being implemented to use the extended covariance data that are now available with the TENDL libraries, but also less often in other ENDF data libraries. There has been substantial validation work. The code is now distributed with a test suite with over 400 test cases, including cross-validation with FISPACT 2007 libraries and tests. Further validation work, such as the decay heat validation study[13], are being actively pursued. Both the random-walk (Section 4) and the Monte-Carlo with model reduction (Section 5) methods are being evaluated.

Covariance data are used to provide better uncertainty predictions. The use of covariance data between different energy groups of a reaction is already fully implemented and tested. The use of covariance data between different reactions is currently being implemented using the approaches described in this paper.

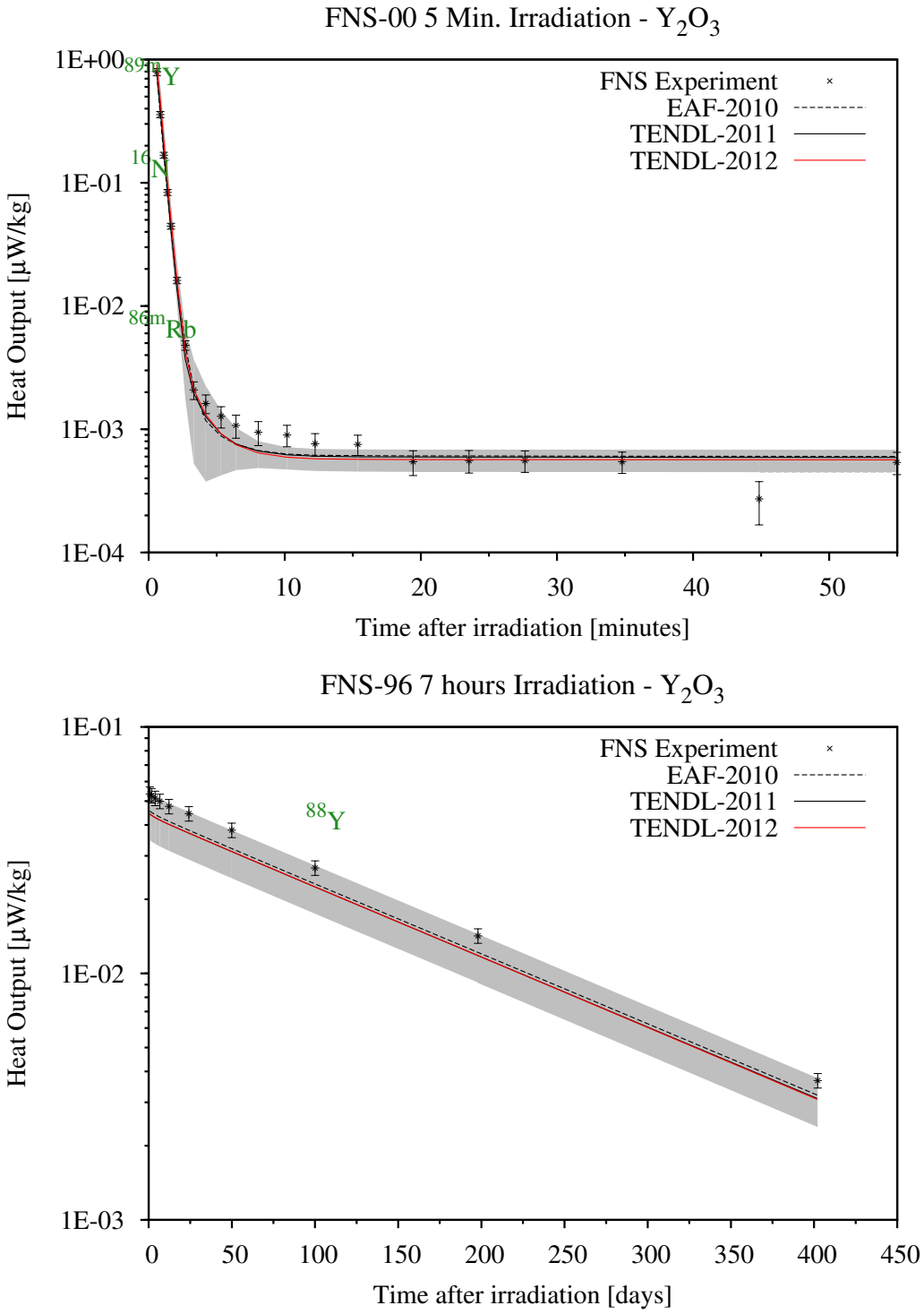

Figure 7. Yttrium oxide C/E decay heat comparison, TENDL derived uncertainty as gray area.

Acknowledgments

This work was undertaken under contract to the UK Atomic Energy Authority (on the RCUK Energy Programme under grant EP/1501045).

REFERENCES

[1] J. Eastwood and J. Morgan. *The FISPACT-II Software Specification Document*. *Technical Report CEM/120504/SD/2 Issue 7*, Culham Electromagnetics (2013).

[2] J.-C. Sublet, J. Eastwood, and J. Morgan. *FISPACT-II(12) User Manual*. *Technical Report CCFE-R(11)11 Issue 4*, CCFE (2013).

[3] "EASY-II European Activiation SYstem." http://www.ccfe.ac.uk/EASY.aspx.

[4] R. Forrest. *FISPACT-2007: User Manual*. *Technical Report UKAEA FUS 534*, EURATOM/UKAEA Fusion Association (2007).

[5] J.-C. Sublet, P. Ribon, and M. Coste-Delclaux. *CALENDF-2010: User Manual*. *Technical Report CEA-R-6277, ISSN 0429-3460*, CEA (2011).

[6] E. Martinho, J. Salgado, and I. Gonçalves. "Universal curve of the thermal neutron self-shielding factor in foils, wires, spheres and cylinders." *J. Radioanal. Nucl. Chem.*, **261(3)**: pp. 637–643 (2004).

[7] J.-C. Sublet *et al.* *The European Activation File: EAF-2010 neutron-induced cross section library*. *Technical Report CCFE-R(10)05*, CCFE (2010).

[8] A. J. Koning and D. Rochman. "TENDL-2012: TALYS-based Evaluated Nuclear Data Library." http://www.talys.eu/tendl-2012 (2012).

[9] A. Koning and D. Rochman. "Modern Nuclear Data Evaluation with the TALYS Code System." *Nuc. Data Sheets*, **113(12)**: pp. 2841–2934 (2012).

[10] M. Herman and A. Trkov, editors. *ENDF-6 Formats Manual, Data Formats and Procedures for the Evaluated Nuclear Data File ENDF/B-VI and ENDF/B-VII*, volume BNL-90365-2009 Rev. 2. Brookhaven National Laboratory (2011).

[11] J. Eastwood. *Using Graph Theory Methods for Enumerating Pathways*. *Technical Report CEM/081203/TN/1*, Culham Electromagnetics (2010).

[12] J. Eastwood and J. Morgan. *Pathways and Uncertainty Prediction in FISPACT-II*. *Technical Report CEM/130516/TN/1*, Culham Electromagnetics. Presented at SNA+MC 2013 (2013).

[13] J.-C. Sublet and M. Gilbert. *Decay heat validation, FISPACT-II & TENDL-2012,-2011 and EAF-2010 nuclear data libraries*. *Technical Report CCFE-R(13)20*, CCFE, UK Atomic Energy Authority, Culham Science Centre, OX14 3DB,UK (2013).

[14] F. Maekawa, M. Wada, and Y. Ikeda. *Decay Heat Experiment and Validation of calculation code systems for fusion reactor*. *Technical Report JAERI 98-055*, JAEA. http://www.jaea.go.jp/jaeri/ (1999).